Journal of Vibration Engineering & Technologies
https://doi.org/10.1007/s42417-023-00967-9

ORIGINAL PAPER

Numerical Analysis of Vibration Attenuation and Bandgaps in Radially Periodic Plates

E. Manconi[1] · **A. Hvatov**[2] · **S. V. Sorokin**[3]

Received: 30 November 2022 / Revised: 15 March 2023 / Accepted: 24 March 2023

Abstract

Objective Periodic configuration of mechanical and civil structures has shown great potential for noise and vibration reduction. However, the use of Cartesian coordinates in studying periodicity effects in elastic structures overlooks the benefits of radially periodic configurations when dealing with wave propagation in large flexible plates disturbed by a small source area. This paper presents an easy-to-use numerical approach to predicting bandgap characteristics in polar coordinates.

Methodology To demonstrate the vibration-attenuation effect, we consider a circular radially periodic plate model. We use an adapted Wave Finite-Element method in numerical experiments to demonstrate the existence of the attenuation effect. To verify the numerical results, we apply an adapted Floquet theory to polar coordinates.

Results and Conclusions Our findings indicate that theoretical and numerical results are in excellent agreement considering a new parameter that introduces the distance from the origin. The adapted Wave Finite-Element approach and Floquet theory presented here demonstrate their potential to model more complex structures in polar coordinates.

Keywords Waves · Finite elements · Plates · Polar periodicity · Periodic structures · Stop-band · Vibration attenuation

Introduction

Periodic structures have the properties to strongly attenuate vibration transmission in specific frequency ranges, called stop-bands [1]. This periodicity effect is often called Bragg scattering effect with reference to the propagation of X-rays in crystalline materials investigated in 1912 by William Lawrence Bragg and William Henry Bragg. Due to its potential applications in noise and vibration harshness mitigation in various engineering areas, modelling periodic structures have become an active and prolific research subject in structural dynamics. The interest has grown with the new technological possibility of creating multi-scale periodic structures with local resonance phenomena, which has made the design of these structures very attractive for new metamaterials [2–4].

Floquet's theorem, applied in 1946 by Brillouin to solve the wave equation [1], is a powerful approach to studying waveguide properties of periodic structures from the knowledge of the dynamic properties of a single period (cell). Since this theorem heavily relies on the translational invariance of the problem formulation, periodicity effects have been studied by its means mainly in Cartesian coordinates, while polar periodicity has very seldom been examined, for example [5–7]. However, many engineering applications deal with structures whose dynamics can be conveniently described in polar coordinates, e.g. flexible membranes or plates of a circular shape, built-up structures with beam/plate connections, large flexible structures locally excited by alternative machines, and so on. In all these cases, radial periodicity can be utilised to reduce vibration transmission, and the periodic inserts can function as a vibroacoustic filter when the dominant excitation frequency falls within a stop-band. The use of radial periodicity for vibration reduction

✉ E. Manconi
elisabetta.manconi@unipr.it

A. Hvatov
alex_hvatov@itmo.ru

S. V. Sorokin
svs@mp.aau.dk

[1] Department of Engineering and Architecture, University of Parma, Parco Area Delle Scienze 181/A, 43100 Parma, Italy

[2] NSS Lab, ITMO University, Kronverksky Pr. 49, Saint-Petersburg 197101, Russia

[3] Department of Materials and Production, Aalborg University, Fibigerstrade 16, 9220 Aalborg, Denmark

Published online: 06 May 2023

was, for example, investigated in [8] where it was shown that a periodic structure, arranged in a stepwise shape along the radial direction, was able to attenuate vibration due to its low-frequency bandgap characteristics. Radial periodic structures have also been shown to be effective in protecting constructions from seismic waves; as an example, in [9], a new type of seismic metamaterial with radial periodicity was studied, demonstrating its effectiveness, compared to traditional seismic metamaterials, in attenuating seismic Lamb and surface waves.

Although a mathematically rigorous reformulation of Floquet's theorem for polar coordinates is problematic, its far-field analogue, known as the theory of Bragg fibre, has been formulated in optics [10–12]. In [7], the Floquet propagator has been introduced as a function of the radial coordinate, and several heuristically chosen approximations of this dependence have been compared with each other and verified via direct numerical integration. The recent paper [13] has addressed the formulation of a propagator, which is equally applicable to Cartesian and polar coordinates. Then its independence upon the axial Cartesian coordinate naturally emerges, and its dependence upon the radial polar coordinate becomes uniquely defined in agreement with findings presented in [7].

The wave and finite-element (WFE) method has now become a classical tool to analyse properties of periodic and authentically uniform waveguides of arbitrary complexity in Cartesian coordinates. It has been presented in many papers and studies, and several benchmark cases have shown its practical applicability to periodic and continuous structures, e.g. [14]. The method models a single period, or cell, using standard finite-element (FE) analysis, and it applies Floquet/Bloch theory [1] to evaluate the behaviour of the whole structure in terms of wave propagation. Recently, the WFE has been generalised to predict free and forced wave propagation in radially periodic plates [15, 16]. In particular, in [15], the response to harmonic excitation was studied close to the excitation zone and in the low-frequency range (in the first pass-band), while in [16], the prediction of vibration attenuation was verified by comparison with standard finite-element analysis of a finite plate. It is of worth mentioning here that stop-bands rigorously occur in infinite periodic structures, while attenuation bands are found in finite structures with the insertion of periodic cells. When the number of inserted periodic cells is large, it has been shown that the attenuation- and stop-bands are the same [17–19].

For consistency, the procedures outlined in [13] and [16] are presented to predict and verify stop-bands and vibration attenuation bands in radially periodic plates. The main advance from [13] and [16] is the generalisation of these procedures for an arbitrary circumferential wavenumber. The paper is organised as follows. In "Floquet Propagator in Polar Coordinates", the formulation of the Floquet propagator, equally applicable to Cartesian and Polar Coordinates, is presented, showing that it can be used to assess the WFE applicability for the identification of pass-bands in periodic plates in the same way as it has been done for membranes in [13]. In "The Wave/Finite Element and Wave Amplitude Decay Prediction", the WFE approximation to model free and forced wave propagation for an arbitrary circumferential wavenumber is described. Only a few segments of a sector of the structure are discretised using conventional FE. Periodicity conditions are applied to develop a WFE polynomial eigenproblem whose solutions yield the wavenumber-frequency relation and wavemodes. These are further used to obtain information on the wave energy flowing and describe the structure's response to localised excitation sources. "Numerical Examples" contains examples, which demonstrate excellent agreement between results obtained using the procedures outlined in [13] and [16] and their verification.

Floquet Propagator in Polar Coordinates

A schematic representation of a polar periodic plate is shown in Fig. 1. The figure shows a plate with repetition both in the circumferential direction, periodic angle α, and in the radial direction, periodic length L. To avoid numerical errors and singularities, the first cell is shifted at an arbitrarily small distance R_0 from the origin of the polar coordinates. The internal radius R_0 is an important novel geometrical parameter (in comparison with the problem formulation in Cartesian coordinates) of the problem.

In this paper, we consider only radially periodic plates. However, since vibrations of these plates feature a circumferential wavenumber $m = 0, 1, 2, \ldots$ as $\cos(m\theta)$, the set of equally spaced rays in Fig. 1 represents radial nodal lines of a vibration mode. In the framework of WFE modelling (see "Floquet Propagator in Polar Coordinates" for details), only one 'slice' of angle α needs to be considered. Then, this angle may not obey the relation $\alpha = \frac{\pi}{m}$ with m being an integer number.

As is well known for periodic structures in Cartesian coordinates, free waves—although purely time-harmonic—become spatially composite, which is clearly seen in their Fourier decomposition [20, 21]. Conversion of the problem formulation and solution to polar coordinates implies the replacement of sine and cosine with Hankel functions. Then, a composite wave in the radially periodic membrane also has a discrete spectrum in Hankel decomposition rather than a single component. As substantiated in [7], formulation of Floquet propagator for such a membrane requires adjustment of its conventional Cartesian formulation using a "cylindrical wave correction factor", which is applied to the whole composite wave whatever its decomposition content.

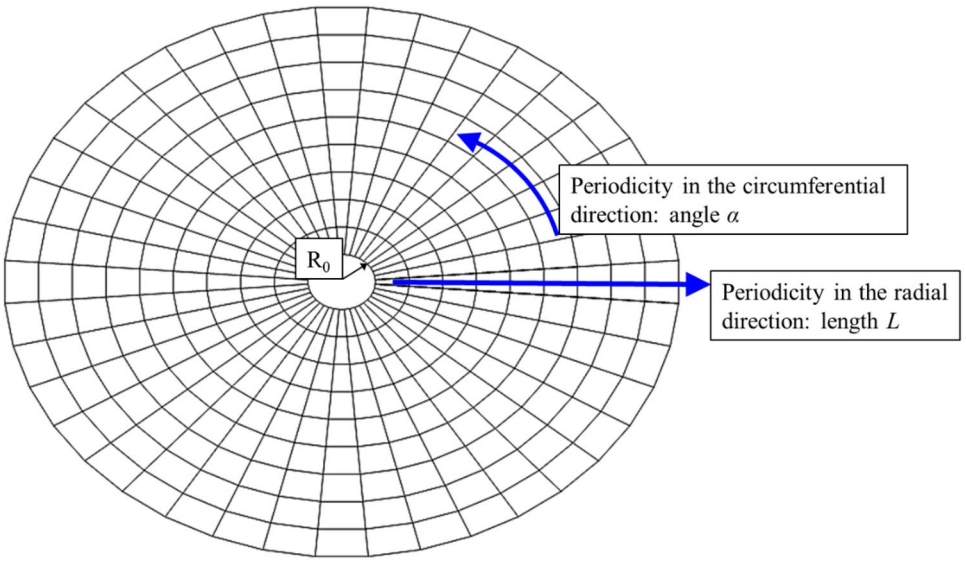

Fig. 1 Schematic representation of the polar periodic plate model

To compare the stop-bands obtained with Floquet theory and the WFE method, we first briefly reproduce all required steps to determine the "cylindrical wave correction", or shape function, for a periodic plate. It is assumed that the dynamics of the plate is governed by the classical Kirchhoff plate equation shown in Eq. (1):

$$D\nabla^4 w - \rho h \frac{\partial^2 w}{\partial t^2} = 0, \tag{1}$$

where D is the bending stiffness expressed as $D = \frac{Eh^3}{12(1-\nu^2)}$ with Young modulus E and Poisson ratio ν. In what follows, we use a time-harmonic state $\exp(-i\omega t)$ and dimensionless frequency parameter $\Omega = \omega L^2\sqrt{\rho h_1 / D_1}$ and we assume that the structure has two parts with parameters $L_i, h_i, D_i, i = 1, 2$ and $L = L_1 + L_2$.

Cartesian Coordinates

For consistency, we reproduce here the classical solution of the one-dimensional "cylindrical bending" problem in Cartesian coordinates. General solutions of Eq. (1) for alternating parts have the form of Eq. (2):

$$w_i(x) = \begin{cases} A^{(i)}\exp(i\sqrt{\Omega}x) + B^{(i)}\exp(-i\sqrt{\Omega}x) + C^{(i)}\exp(\sqrt{\Omega}x) + D^{(i)}\exp(-\sqrt{\Omega}x) \\ \qquad , x \in \text{first part} \\ A^{(i)}\exp(i\sqrt{\frac{\Omega}{\sigma}}x) + B^{(i)}\exp(-i\sqrt{\frac{\Omega}{\sigma}}x) + C^{(i)}\exp(\sqrt{\frac{\Omega}{\sigma}}x) + D^{(i)}\exp(-\sqrt{\frac{\Omega}{\sigma}}x) \\ \qquad , x \in \text{second part} \end{cases} \tag{2}$$

For simplicity, we use dimensionless parameter $\sigma = \sqrt{\frac{h_2 D_1}{h_1 D_2}}$ in Eq. (2). To impose continuity of the structure, interfacial conditions are used as in Eq. (3):

$$\begin{aligned} w_i(L_1) &= w_{i+1}(L_1)\,; & w_{i+1}(L_1+L_2) &= w_{i+2}(L_1+L_2); \\ w_i'(L_1) &= w_{i+1}'(L_1); & w_{i+1}'(L_1+L_2) &= w_{i+2}'(L_1+L_2); \\ M_i(L_1) &= \sigma M_{i+1}(L_1)\,; & \sigma M_{i+1}(L_1+L_2) &= M_{i+2}(L_1+L_2); \\ Q_i(L_1) &= \sigma Q_{i+1}(L_1); & \sigma Q_{i+1}(L_1+L_2) &= Q_{i+2}(L_1+L_2); \end{aligned} \tag{3}$$

where $M = w''(x)$ and $Q = w'''(x)$ are the bending moment and shear force, respectively.

Using classical guidelines, we use periodicity conditions from Eq. (4):

$$\begin{aligned} &[w_i(x) - \Lambda w_{i+2}(x+L)]\big|_{x=x_0} = 0; \\ &\frac{\partial}{\partial x}[w_i(x) - \Lambda w_{i+2}(x+L)]\big|_{x=x_0} = 0; \\ &\frac{\partial}{\partial x^2}[w_i(x) - \Lambda w_{i+2}(x+L)]\big|_{x=x_0} = 0; \\ &\frac{\partial}{\partial x^3}[w_i(x) - \Lambda w_{i+2}(x+L)]\big|_{x=x_0} = 0. \end{aligned} \tag{4}$$

Obviously, the last two equations formulate periodicity of bending moments and shear forces. In Eq. (4), point x_0

could be chosen arbitrarily due to the translational symmetry of operator in Eq. (1) in Cartesian coordinates. Furthermore, in Eq. (4), we introduce the Floquet propagator Λ, which is linked to the classical Bloch's propagation constant as $\Lambda = \exp(iK_B)$. To find Λ, we substitute Eq. (2) into Eqs. (3) and (4) and obtain a system of eight linear algebraic equations with respect to modal amplitudes. The resulting determinant is the fourth-order polynomial in Λ and has the form

$$D(\Lambda, \Omega) = \Lambda^4 + a_3(\Omega)\Lambda^3 + a_2(\Omega)\Lambda^2 + a_1(\Omega)\Lambda + 1 = 0 \tag{5}$$

In the following subsection, we show briefly how the classical Cartesian formulation is modified to obtain the Floquet propagator in polar coordinates.

Polar Coordinates

In polar coordinates, the general solution of Eq. (1) acquires a form of a linear combination of Bessel functions of the same integer order, which defines the circumferential wavenumber. Therefore, solutions for alternating parts are

$$w_i(r) = \begin{cases} A^{(i)}H_m^{(1)}(\Omega r) + B^{(i)}H_m^{(2)}(\Omega r) + C^{(i)}I_m(\Omega r) + D^{(i)}K_m(\Omega r), \ r \in \text{first part} \\ A^{(i)}H_m^{(1)}(\frac{\Omega}{\sigma} r) + B^{(i)}H_m^{(2)}(\frac{\Omega}{\sigma} r) + C^{(i)}I_m(\frac{\Omega}{\sigma} r) + D^{(i)}K_m(\frac{\Omega}{\sigma} r), \ r \in \text{second part} \end{cases} \tag{6}$$

In Eq. (6), $H_m^{(j)}$, $j = 1, 2$ are the Hankel functions of first and second kind of order m and I_m, K_m are modified Bessel functions of order m. Following the Cartesian guideline proposed in "Cartesian Coordinates", we use interfacial conditions to preserve the continuity of the system. However, the operator in Eq. (1) does not have translational symmetry in polar coordinates in contrast with the Cartesian case. Moreover, in contrast to the canonical formulation in Cartesian coordinates, periodicity conditions and propagator become dependent upon an initial hole size R_0 [7]. Therefore, the classical mathematically rigorous formulation of the Floquet propagator $\Lambda = \exp(iK_B)$ with Bloch's constant becomes inapplicable and requires a modification.

Starting from interfacial conditions, all equations should contain R_0 as a parameter. Thus, the resulting interfacial conditions have a different form from Eq. (3) and they are defined as shown in Eq. (7):

$$\begin{aligned} w_i(R_0 + L_1) &= w_{i+1}(R_0 + L_1); & w_{i+1}(R_0 + L_1 + L_2) &= w_{i+2}(R_0 + L_1 + L_2); \\ w_i'(R_0 + L_1) &= w_{i+1}'(R_0 + L_1); & w_{i+1}'(R_0 + L_1 + L_2) &= w_{i+2}'(R_0 + L_1 + L_2); \\ M_i(R_0 + L_1) &= \sigma M_{i+1}(R_0 + L_1); & \sigma M_{i+1}(R_0 + L_1 + L_2) &= M_{i+2}(R_0 + L_1 + L_2); \\ Q_i(R_0 + L_1) &= \sigma Q_{i+1}(R_0 + L_1); & \sigma Q_{i+1}(R_0 + L_1 + L_2) &= Q_{i+2}(R_0 + L_1 + L_2); \end{aligned} \tag{7}$$

where

$$M = w''(r) + \nu\left(\frac{1}{r}w'(r) - \frac{m^2}{r^2}w\right)$$

and

$$Q = w'''(r) + (2-\nu)\left(\frac{1}{r}w'' + \frac{1}{r^2}w'(r) - \frac{m^2}{r^2}w'(r) + 2\frac{m^2}{r^3}w(r)\right)$$

are the bending moment and shearing force, respectively.

Periodicity conditions and propagator should be functions of the initial hole size R_0, and the modified periodicity conditions have the form

$$\begin{aligned} &[w_i(r) - \Lambda(r)w_{i+2}(r+L)]\big|_{r=R_0} = 0; \\ &\frac{\partial}{\partial r}[w_i(r) - \Lambda(r)w_{i+2}(r+L)]\big|_{r=R_0} = 0; \\ &\frac{\partial}{\partial r^2}[w_i(r) - \Lambda(r)w_{i+2}(r+L)]\big|_{r=R_0} = 0; \\ &\frac{\partial}{\partial r^3}[w_i(r) - \Lambda(r)w_{i+2}(r+L)]\big|_{r=R_0} = 0. \end{aligned} \tag{8}$$

The exact equation to find the propagator is obtained by substituting Eq. (6) in Eqs. (7) and (8). As substantiated in [7] and [13], the resulting determinant is a fourth-order polynomial in Λ:

$$\begin{aligned} D(\Lambda, \Omega) = \Lambda(R_0)^4 + a_3(R_0, \Omega)\Lambda(R_0)^3 + a_2(R_0, \Omega)\Lambda(R_0)^2 \\ + a_1(R_0, \Omega)\Lambda(R_0) + a_0(R_0, \Omega) = 0. \end{aligned} \tag{9}$$

The difference from the Cartesian case is that coefficient $a_0(R_0, \Omega)$ is not constant. Therefore, we modify Floquet theory as shown in [13] with the assumption $\Lambda(R_0) = S(R_0)\Lambda$, where $S(R_0)$ is the shape function. The latter is obtained from equation $a_0 \equiv 1$ and has the form

$$S(R_0) = \pm\sqrt{1 + L/R_0}, \tag{10}$$

which matches the "cylindrical wave-correction" function for a homogeneous plate [13]. Moreover, the same shape function appears for the homogeneous and periodic membrane. Then the propagator for a periodic plate in polar coordinates is $\Lambda(R_0) = \tilde{\Lambda}(R_0)\sqrt{1 + L/R_0}$. The condition

$\Lambda(R_0) = \tilde{\Lambda}(R_0)\sqrt{1+\tau/R_0}$ defines the location of pass-bands. However, for a homogeneous membrane, the opposite case, $\left|\tilde{\Lambda}_1(R_0)\right| = \left|\tilde{\Lambda}_2(R_0)\right| = 1$, does not necessarily specify a stop-band zone if these propagators are computed in the immediate vicinity of the origin of coordinate system.

Nevertheless, introduction of the shape function $S(R_0)$ permits to unify the formulation of propagators in Cartesian and polar coordinates and recovers the conventional criterion of stop-band formation $\left|\tilde{\Lambda}_1(R_0)\right| \neq \left|\tilde{\Lambda}_2(R_0)\right| \neq 1$ "almost everywhere" in the (Ω, R_0) plane. This result, known for a membrane model [13], is now generalised for the model of a plate, which, on top of propagating cylindrical waves, captures evanescent ones.

The Wave/Finite Element and Wave Amplitude Decay Prediction

Compared to the corresponding Cartesian periodic structure, in polar periodic structures, the wave amplitude attenuation is dependent upon the distance from the centre. Following the procedure in [16], this section presents how to model this decay for free and forced wave propagation using the WFE formulation.

Continuous structures can be studied using this approach but assuming arbitrary periodic spatial discretisation [15]. With reference to Fig. 1, if the plate is homogenous in the circumferential direction—radially periodic—the angle α can be assumed to be arbitrarily small; if the plate is homogenous, non-periodic, both arbitrary small length L and angle α are assumed.

A periodic slice of the plates is taken, and it is approximated by a finite number of piecewise rectangular waveguide as shown in Fig. 2. We assume that the periodic angle α is small, so that the properties of the slice do not vary rapidly in the radial direction. The segments in Fig. 2, the unit cells of characteristics length L in the radial direction, are univocally identified by an integer number $j = 1 \ldots n$, representing the cell's radial position.

To apply the method, a unit cell j is taken and meshed using conventional FE analysis as in Fig. 2. The cell can be of complicated construction and with internal nodes. These are condensed and reduced to obtain a super-element, whose nodal degrees are ordered as $\mathbf{q}_L = \left\{\mathbf{q}_1^T \;\; \mathbf{q}_2^T\right\}^T$ and $\mathbf{q}_R = \left\{\mathbf{q}_3^T \;\; \mathbf{q}_4^T\right\}^T$. Here $\mathbf{q}_R = \left\{\mathbf{q}_3^T \;\; \mathbf{q}_4^T\right\}^T$ and $\mathbf{q}_L$ are the Degrees of Freedom (DOFs) at the left and right sides of the unit cell. The figure also shows that local coordinates can be rotated, by the angle α, to model the desired curvature as in [22, 23]. The WFE method has been introduced in many papers, e.g. [14, 15, 22–25], and it is not detailed here. For completeness, an overview of the method is given in the Appendix A. Compared to [16], the formulation in the Appendix is given for 1- and 2-dimensional axisymmetric structures. The latter allows the evaluation of circular plate modes separately.

Since the full libraries of commercial FE software can be used, the approach is not limited to thin circular or annular circular plates, but it can be equally applied to laminated, composite and thick plates using either 2D or 3D solid finite elements' formulation without more effort. Moreover, the inclusion of curvature, stress, temperature effects and damping in the model can be accommodated, if necessary, as described in [23].

For each segment j, complex dispersion curves, $(\mathbf{k}_j, \omega)$, nodal displacements $\mathbf{\Phi}_{j\mathbf{q}}$ (wave modes) and nodal forces $\mathbf{\Phi}_{j\mathbf{f}}$, which occur under the passage of a wave, are obtained as described in Appendix A. Using these wavemodes as basis functions, the total nodal displacements and forces of a segment j can be expanded by the sum of a finite number of the positive and negative wavemodes so that

$$\begin{bmatrix} \mathbf{q}_{jL} \\ \mathbf{f}_{jL} \end{bmatrix} = \begin{bmatrix} \mathbf{\Phi}_{j\mathbf{q}}^{+} & \mathbf{\Phi}_{j\mathbf{q}}^{-} \\ \mathbf{\Phi}_{j\mathbf{f}}^{+} & \mathbf{\Phi}_{j\mathbf{f}}^{-} \end{bmatrix} \begin{bmatrix} \mathbf{a}_j^{+} \\ \mathbf{a}_j^{-} \end{bmatrix}, \tag{11}$$

where $\mathbf{a}$ is the wave amplitude and the + and – superscripts refer to positive and negative propagating waves [14, 24].

An external disturbance, force or displacement, is applied to the left DOFs of the segment $j = 1$. Therefore, only positive going waves of amplitude $\mathbf{a}^{+}$, propagating away from the excitation point, will be generated. As an example, if an external force $\mathbf{\Phi}_{1\mathbf{f}}^{+}\mathbf{a}_1^{+} = \mathbf{f}_e$ is applied, the excited wave amplitudes will be obtained from

$$\mathbf{\Phi}_{1\mathbf{f}}^{+}\mathbf{a}_1^{+} = \mathbf{f}_e, \tag{12}$$

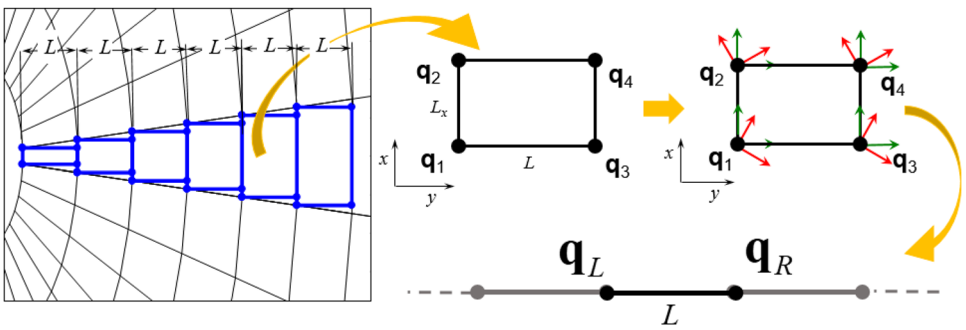

Fig. 2 Approximation of a periodic polar plate by a piecewise Cartesian waveguide and WFE discretisation of the unit cell j

see Eq. (9) in [14]. To recover $\mathbf{a}_1^+$, instead of using pseudo-inversion, it is advantageous to exploit the left eigenvectors of the WFE eigenvalue problem to avoid numerical issues. For the segment j, the left eigenvectors are denoted as

$$\mathbf{\Psi}_j = \begin{bmatrix} \mathbf{\Psi}_{j\mathbf{f}}^+ & \mathbf{\Psi}_{j\mathbf{q}}^+ \\ \mathbf{\Psi}_{j\mathbf{f}}^- & \mathbf{\Psi}_{j\mathbf{q}}^- \end{bmatrix}, \tag{13}$$

Left eigenvectors are orthogonal to the wavemodes and can be normalised, $\mathbf{\Psi\Phi} = \mathbf{I}$. Therefore, the excited wave amplitude for the first segment $j = 1$ is obtained by

$$\mathbf{a}_1^+ = \mathbf{\Psi}_{1\mathbf{q}}^+ \mathbf{f}_e. \tag{14}$$

Once the forced wave amplitudes in the first segment are found, the wave amplitudes in the next segment can be predicted as follows. Since we are considering a lossless waveguide with slowly varying geometrical properties, we can assume that the power associated with each propagating wave is preserved along the waveguides.

In the corresponding Cartesian waveguide, the nodal displacements and forces between two adjacent cells are related by the periodicity conditions

$$\mathbf{q}_{(j+1)L} = \mathbf{\Lambda}_j^+(L)\mathbf{q}_{jL} \text{ and } \mathbf{f}_{(j+1)L} = \mathbf{\Lambda}_j^+(L)\mathbf{f}_{jL} \tag{15}$$

where $\mathbf{\Lambda}_j^+(L) = \text{diag}\left[\exp(-i\mathbf{k}_j^+ L)\right]$ is the diagonal matrix with Bloch's propagation constant

Using Eqs. (11)–(15), the left nodal displacements and forces of the unit cell $j+1$ are recovered from

$$\begin{aligned} \mathbf{q}_{(j+1)L} &= \mathbf{\Lambda}_j^+(L)\mathbf{\Phi}_{j\mathbf{q}}^+ \mathbf{a}_j^+; \\ \mathbf{f}_{(j+1)L} &= \mathbf{\Lambda}_j^+(L)\mathbf{\Phi}_{j\mathbf{f}}^+ \mathbf{a}_j^+. \end{aligned} \tag{16}$$

Using the left eigenvectors as in Eq. (14), the first estimation of the wave amplitudes in the $j+1$ cell is obtained from

$$\tilde{\mathbf{a}}_{(j+1)}^+ = \mathbf{\Psi}_{(j+1)\mathbf{f}}^+ \mathbf{q}_{(j+1)L} + \mathbf{\Psi}_{(j+1)\mathbf{q}}^+ \mathbf{f}_{(j+1)L}. \tag{17}$$

In a uniform and lossless waveguide, the amplitudes of waves propagating in the structure do not change. This is not true in non-uniform waveguides, where the wave amplitudes are a function of the position. In particular, in our case, we are considering a lossless waveguide with slowly varying geometrical properties—due to the assumption of small angles α—and we can assume that the power associated with each propagating wave is preserved along the waveguides. The time-average energy flow density in each segment j can be evaluated from

$$\Pi_j = \frac{1}{2}\mathbf{f}_{jL}^H \dot{\mathbf{q}}_{jL} = \frac{1}{2}\mathbf{f}_{jL}^H i\omega \mathbf{q}_{jL},$$

where the superscript H denotes the Hermitian transpose. This energy flow is complex-valued [26]: its real part, $\text{Re}(\Pi_j)$, being the average power; its imaginary part, $\text{Im}(\Pi_j)$, being the peak of the reactive power, which can be seen as the stored averaged energy density in analogy with circuit theory.

The wave amplitudes change, due to the changes in the geometry, can be accommodated by requiring that the time-average energy flow density through the interfaces of each Cartesian segment is the same [25]. Therefore, we deduce that the ratio between $\text{Re}(\Pi_j)$ and $\text{Re}(\Pi_{j+1})$ gives the wave amplitude decay $\xi_{(j+1)}$:

$$\xi_{(j+1)}^2 = \frac{\text{Re}(\Pi_j)}{\text{Re}(\Pi_{(J+1)})} = \frac{\text{Re}\left\{\mathbf{f}_{jL}^H i\omega \mathbf{q}_{jL}\right\}}{\text{Re}\left\{\mathbf{f}_{(i+1)L}^H i\omega \mathbf{q}_{(j+1)L}\right\}} \rightarrow \mathrm{a}_{(j+1)}^+ = \xi_{(j+1)}\tilde{\mathrm{a}}_{(j+1)}^+ \tag{18}$$

Once the wave amplitude change is evaluated, the nodal displacements and forces of the next segment can be predicted as

$$\begin{aligned} \mathbf{q}_{(j+1)L} &= \mathbf{\Lambda}_{(j+1)}^+(L)\mathbf{\Phi}_{(j+1)\mathbf{q}}^+ \xi_{(j+1)}\tilde{\mathbf{a}}_{(j+1)}^+; \\ \mathbf{f}_{(j+1)L} &= \mathbf{\Lambda}_{(j+1)}^+(L)\mathbf{\Phi}_{(j+1)\mathbf{f}}^+ \xi_{(j+1)}\tilde{\mathbf{a}}_{(j+1)}^+. \end{aligned} \tag{19}$$

The same passages are repeated to obtain the displacements and nodal forces at the target radial distance.

In the stop-bands, where only evanescent and highly decaying waves exist, there is no significant energy flow but mainly reactive power and

$$\begin{aligned} \mathbf{q}_{(j+1)L} &= \mathbf{T}_{(j+1)}^+(L)\mathbf{\Phi}_{(j+1)\mathbf{q}}^+ \xi_{(j+1)}\tilde{\mathbf{a}}_{(j+1)}^+; \\ \mathbf{f}_{(j+1)L} &= \mathbf{T}_{(j+1)}^+(L)\mathbf{\Phi}_{(j+1)\mathbf{f}}^+ \xi_{(j+1)}\tilde{\mathbf{a}}_{(j+1)}^+. \end{aligned}$$

Notice that the same considerations hold if the waves are travelling towards the centre of the plate, but the wave amplitude growth will be given by the reciprocal of Eq. (18).

Numerical Examples

In this section, a numerical example of a plate with periodically varying thickness is presented. Figure 3 depicts a schematic representation of the plate with annuli of different

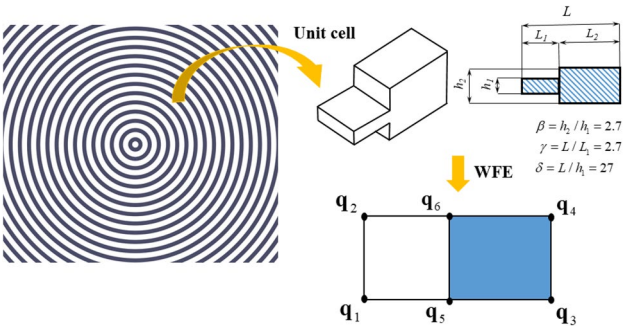

Fig. 3 Schematic representation of an infinite plate with periodically varying thickness, its unit cell, and WFE model

thickness. The unit cell and its WFE super-element are also shown.

The material properties are: Young's modulus 210 GPa, density 7850 kg/m^3 and Poisson's ratio 0.3. The non-dimensional frequency $\Omega = \omega L^2\sqrt{\rho h_1 / D_1}$ is introduced, where ρ, h_1 and D_1 are the density, thickness and bending stiffness of the corresponding homogeneous plate of thickness h_1, and ω is the frequency in radiant. The geometrical characteristics of the unit cell are indicated in Fig. 3.

The nodal degrees of freedom $\mathbf{q}$ of the cell in Fig. 3 are ordered as $\mathbf{q} = \left[\mathbf{q}_L^T \ \mathbf{q}_R^T \ \mathbf{q}_I^T\right]^T$, where *L, R* and *I* are associated with the right, left and interior nodal degrees of freedom of the cell, with a similar expression for the nodal forces. In this case, the discretised equation of motion, $\mathbf{Dq} = \mathbf{f}$ is partitioned as

$$\begin{bmatrix} \mathbf{D}_{LL} & \mathbf{D}_{LR} & \mathbf{D}_{RI} \\ \mathbf{D}_{RL} & \mathbf{D}_{RR} & \mathbf{D}_{RI} \\ \mathbf{D}_{IL} & \mathbf{D}_{IR} & \mathbf{D}_{II} \end{bmatrix} \begin{Bmatrix} \mathbf{q}_L \\ \mathbf{q}_R \\ \mathbf{q}_I \end{Bmatrix} = \begin{Bmatrix} \mathbf{f}_L \\ \mathbf{f}_R \\ \mathbf{f}_I \end{Bmatrix}. \tag{20}$$

The internal DoFs of the unit cell must be reduced as described in [27]. Dynamic condensation can be applied, viz. $\mathbf{q}_I = -\mathbf{D}_{II}^{-1}\left(\mathbf{D}_{IL}\mathbf{q}_L + \mathbf{D}_{IR}\mathbf{q}_R\right)$, or other more efficient condensing approaches can be considered, e.g. [27].

Bandgap Analysis and Verification

Bandgaps can be clearly represented using dispersion diagrams. In particular, stop-bands occur when there are no propagating waves and, for lossless waveguides, the absolute value of the propagation is not equal to one, viz. $|\lambda| = \left|e^{-ikL}\right| \neq 1$. Using the material parameters from "Numerical Examples" and Eqs. (6)–(8) together with the shape from Eq. (10), we can determine theoretical stop-bands for different values of initial hole radius R_0 as shown in Fig. 4a.

The Cartesian periodic Kirchhoff plate stop-bands are naturally recovered at the limit $R_0 \to \infty$. However, as seen in this figure, their convergence to the Cartesian stop-band is very fast—already at $R_0 = L$ there is virtually no difference between locations of "polar" and "Cartesian" stop-band. For $R_0 < L$ polar, Floquet propagator predicts location of the left border of this stop-band with reasonable accuracy, whereas the frequency of its right border is much higher than its Cartesian counterpart. It should be noticed that, as discussed in "Floquet Propagator in Polar Coordinates", conditions $\left|\tilde{\Lambda}_1(R_0)\right| = \left|\tilde{\Lambda}_2(R_0)\right| = 1$ do not define in radially periodic plate stop-bands when $R_0 << L$. To verify the positions of stop-bands predicted using Floquet propagator with cylindrical wave correction, a forcing problem should be solved; see [7]. We do not address it here because we aim to compare two alternative approaches to the identification of stop-bands. Figure 4b shows the first bandgap of the radial periodic plate obtained using the WFE approach and the Floquet theory described in "Floquet Propagator in Polar Coordinates" when the distance from the centre of the plate is $R_0 = L$. For values of $R_0 > L$, no significant differences are observed, while for values of $R_0 < L$ the WFE model cannot provide accurate results due to the ratio between the sides of the unit cell, which result in FE mesh distortion errors in this example.

In radially periodic plates, cylindrical waves feature dependence upon angular coordinate theta as $\cos(m\theta)$ with a circumferential wavenumber $m = 0, 1, 2, \ldots$ Figure 5a shows how the theoretical first stop-band varies for different circumferential modes and different R_0.

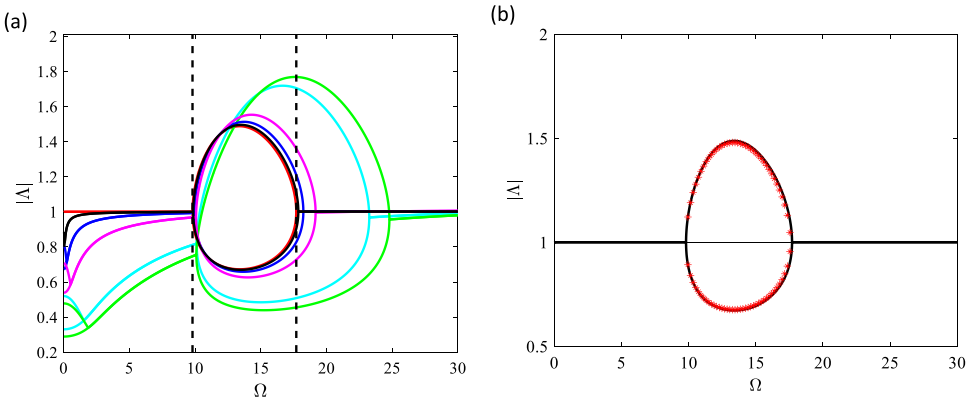

Fig. 4 First stop-band for different internal hole size R_0. **a** Theoretical first stop-bands from Floquet theory ($|\Lambda(R_0)|$ are plotted) in "Floquet Propagator in Polar Coordinates"; ——— $R_0 = 10L$; ——— $R_0 = L$; ——— $R_0 = 0.5L$; ——— $R_0 = 0.27L$; ——— $R_0 = 0.1L$; ——— $R_0 = 0.08L$; — — — Kirchhoff plate. **b** Comparison between the WFE results and the Floquet theory in "Floquet Propagator in Polar Coordinates" for $R_0 = L$ ——— : Floquet formulation; ✱✱✱✱ WFE results

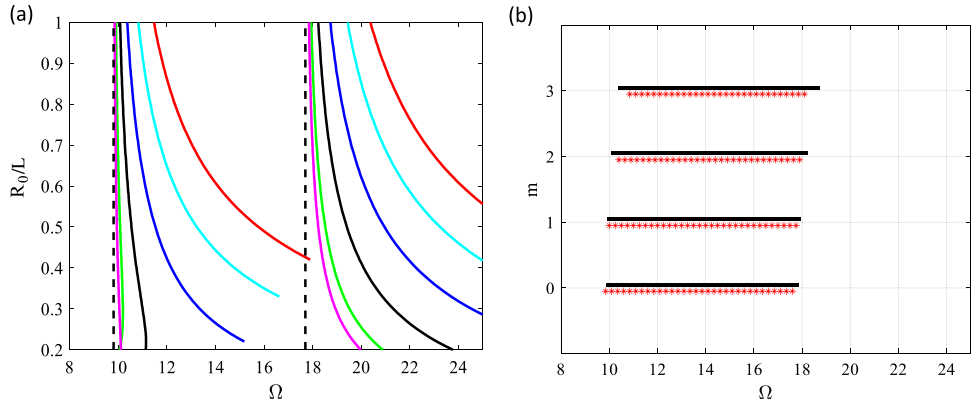

Fig. 5 First stop-band for different circumferential modes m. **a** Theoretical first stop-bands for varying R_0 from Floquet theory ($|\Lambda(R_0)|$ are plotted) in "Floquet Propagator in Polar Coordinates": m=0; m=1; m=2; m=3; m=4; m=5; Kirchhoff plate; **b** Comparison between the WFE stop-bands and the Floquet theory stop-bands in "Floquet Propagator in Polar Coordinates" for $R_0=L$: Floquet formulation; WFE results

As the circumferential mode order increases, while R_0 remains small, the position of the first stop-band strongly shifts towards higher frequencies. However, all stop-bands converge to the Cartesian limit as the initial hole radius grows. It is hardly surprising because the cylindrical wave correction factor, Eq. (10), does not depend upon the circumferential wavenumber. Similarly to the case illustrated in Fig. 4, a forcing problem should be solved to validate these results. However, we are interested in the comparison of Floquet and WFE predictions. Figure 5b depicts the comparison of the first stop-bands for $R_0=L$ and different values of m using the Floquet theory in "Floquet Propagator in Polar Coordinates" and the WFE approach in "The Wave/Finite Element and Wave Amplitude Decay Prediction". It can be seen that the differences in the results increase with the circumferential number. This is due to the differences in the models: Floquet theory in "Floquet Propagator in Polar Coordinates" assumes a classical theoretical approach for separating circumferential modes, while the WFE approximates the phase of change of a wave as it propagates around the circumference using Eq. (A.6) in the Appendix, see also [22].

Of course, plate periodicity generates many stop-bands. However, this subsection has been concerned only with the study of the location of the first stop-band in a radially periodic plate. The reason for this limitation is that, in the first place, we are interested in comparison of results, obtained using the alternative methods. On top of that, as frequency grows, wavelengths in constituents of a radially periodic plate become shorter and, therefore, "far-field" (where the difference between plane and cylindrical waves becomes invisible) emerges (i) at lower frequencies and (ii) closer to the origin of coordinates. This suggests that the location of high-order stop-bands in a radially periodic plate is very close to their Cartesian positions. Finally, advancing to high frequencies makes the applicability of the elementary Kirchhoff plate theory questionable, whereas a use of Timoshenko-Mindlin plate theory lies out of the scope of this paper.

Vibration Response and Attenuation to Local Harmonic Excitation

Vibration response of the radially periodic plate excited by a point force was analysed in [16] using the WFE approach, and the results were verified by comparison with those obtained by standard FEA of a correspondent finite periodic plate modelled in COMSOL Multiphysics®.

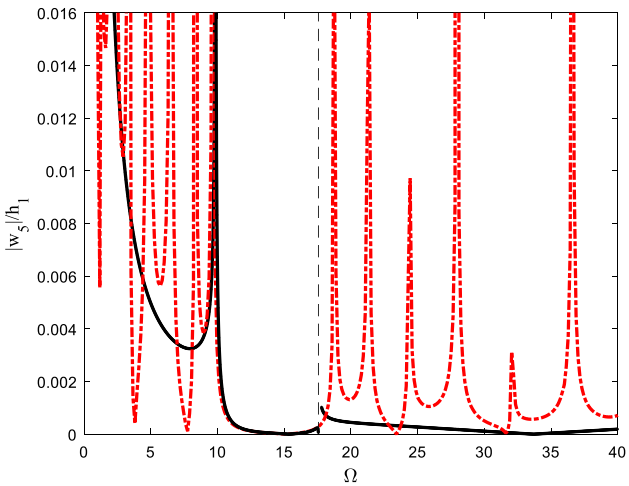

Fig. 6 Forced response $|w_5(\Omega)|/h_1$ from [12]. Comparison between the WFE model and a standard FE model of a finite plate with eight periodic annuli. : WFE results; : FE results. Thin vertical dashed lines show the stop-band in Fig. 4

The FE model was a homogeneous circular plate of thickness h_1 and total radial dimension $R = 10L$, to which periodic annuli were inserted from $R_0 = L$. The plate was assumed to be free. We reproduce these results in Fig. 6, where the absolute value of the transverse response (nodal displacement in the z-direction) is evaluated after the insertion of 5 periodic cells, at a distance $r = 6L$ from the centre of the plate. As expected, few unit cells were enough to obtain a good vibration attenuation in the stop-band, even if the structure is finite.

The stop-band predicted using WFE method is located exactly at the place found using Floquet propagators with cylindrical wave correction; see Fig. 4b. In Fig. 6, this position is confirmed by a significant vibration attenuation in the stop-band detected by means of both the WFE and the standard FE models. The analysis of the response showed one of the main advantages of the WFE approach compared to standard FE approach: incredible reduction of the design and computational time due to the simplified structure and the significantly reduced size of the model. In this case study, for example, the size of the WFE model was a 12×12 matrix after the dynamic reduction, resulting in a WFE model of 6 DOFs, while the FE model was realised using 300364 triangular shell elements.

As seen in Fig. 5b, the location of the stop-band is weakly dependent upon the circumferential wavenumber m. Thus, the response to the time-harmonic excitation circumferentially distributed as $\cos(m\theta)$, $m = 1,2,3$, remains qualitatively the same as for $m = 0$ (which is shown in Fig. 6) and is not presented.

Concluding Remarks

The reported results are summarised as follows:

- The method of Floquet propagators with cylindrical wave correction and the WFE method are in a good agreement with each other in assessing location of stop-bands in radially periodic plates. Both methods, however, should be used for modelling of dynamics of a unit radial periodicity cell positioned at a distance, larger than its length, from the origin of polar coordinates.
- Formulation of Floquet propagators with cylindrical wave correction for identification of stop-bands in radially periodic plates extends the theory of Bragg fibre to waveguides with constituents supporting both propagating and evanescent waves. Therefore, the method of Floquet propagators with cylindrical wave correction may be used for stop-band identification in a broad range of two-dimensional problems in polar and cylindrical coordinates, including high-order plate theories.
- Given the versatility of WFE method with respect to the library of available finite elements, its adjustment to deal with periodicity in polar coordinates facilitates its application for design and optimisation of modern acoustic metamaterials, featuring discrete and continuous constituents in spider net-shaped and similar arrays or lattices.

Advancing with coupled radial/circumferential periodicity in two-dimensional periodic systems and generalisation of both methods to study spherically periodic three-dimensional systems constitute the subjects of our ongoing work.

Appendix

Appendix A

The use of the WFE method to determine dispersion curves and the corresponding wave mode shapes for uniform one-dimensional waveguides is described for example in [14]. A brief overview of the method is given here. Numerical issues related to the application of the method are discussed in [28].

1D Formulation

Waves propagating in the radial direction are considered. With reference to Fig. 4, the nodal degrees of freedom of the segment j are ordered as $\mathbf{q}_L = \left\{\mathbf{q}_1^T \;\; \mathbf{q}_2^T\right\}^T$ and $\mathbf{q}_R = \left\{\mathbf{q}_3^T \;\; \mathbf{q}_4^T\right\}^T$, where $\mathbf{q}_L$ and $\mathbf{q}_R$ are the DOFs at the left and the right side of the segment, with a similar expression for the nodal forces. In the frequency domain, the discretised FE equation of motions of the segment is

$$\left(\mathbf{K} - \omega^2\mathbf{M}\right)\mathbf{q} = \mathbf{D}\mathbf{q} = \mathbf{f} \;\Rightarrow\; \begin{bmatrix} \mathbf{D}_{LL} & \mathbf{D}_{LR} \\ \mathbf{D}_{RL} & \mathbf{D}_{RR} \end{bmatrix} \begin{Bmatrix} \mathbf{q}_L \\ \mathbf{q}_R \end{Bmatrix} = \begin{Bmatrix} \mathbf{f}_L \\ \mathbf{f}_R \end{Bmatrix}, \tag{A.1}$$

in which $\mathbf{M}$ and $\mathbf{K}$ are the mass and stiffness matrices of the segment, and $\mathbf{D}$ is the dynamic matrix of the segment partitioned according to the left and right DOFs.

The relationship between the DOFs at the left- and right-hand sides of the segment is given by

$$\mathbf{q}_R = \lambda\mathbf{q}_L, \tag{A.2}$$

where $\lambda = e^{-ikL}$ and k is the wavenumber. The nodal forces are governed by the equilibrium conditions, so that

$$\left[\mathbf{I}\,\lambda^{-1}\mathbf{I}\right]\mathbf{f} = \mathbf{0}. \tag{A.3}$$

Substituting Eq. (A.2) into Eq. (A.1), and premultiplying both sides of Eq. (A.1) by the matrix $[\mathbf{I} \quad \lambda^{-1}\mathbf{I}]$ in Eq. (A.3), the equation of free wave motion takes the form of a quadratic eigenvalue problem as

$$\left[\lambda^2 \mathbf{D}_{\mathrm{LR}} + \lambda\left(\mathbf{D}_{\mathrm{LL}} + \mathbf{D}_{\mathrm{RR}}\right) + \mathbf{D}_{\mathrm{RL}}\right] \mathbf{q}_{\mathrm{L}} = 0 \tag{A.4}$$

whose solutions yield the relationship between the wavenumber and frequency (dispersion curves) and the displacement $\mathbf{q}_L$ (wave mode shapes) of the cross-section due to wave motion.

2D Formulation for Axisymmetric Structures

In this formulation, the projections k_α and k_r of the wavenumbers k in the radial and circumferential directions are considered. Imposing the periodicity conditions, the nodal DOFs $\mathbf{q} = \left\{ \mathbf{q}_1^T \ \mathbf{q}_2^T \ \mathbf{q}_3^T \ \mathbf{q}_4^T \right\}^T$ on each side of the segment in Fig. 3 are related as

$$\mathbf{q}_2 = \lambda_\alpha \mathbf{q}_1, \ \mathbf{q}_3 = \lambda_y \mathbf{q}_1, \ \mathbf{q}_4 = \lambda_\alpha \lambda_y \mathbf{q}_1 \tag{A.5}$$

where $\lambda_\alpha = e^{-ik_\alpha \alpha}$ and $\lambda_r = e^{-ik_r L}$. Since the angle α is assumed to be small and the phase change of a wave as it propagates around the circumference must be a multiple of 2π, it must be

$$\lambda_\alpha = e^{-in\alpha}. \tag{A.6}$$

Considering that λ_α is known for each circumferential order n, the problem is reduced to a 1D problem and the formulation presented in the first part of the appendix applies.

Funding Open access funding provided by Università degli Studi di Parma within the CRUI-CARE Agreement.

Declarations

Conflict of Interest On behalf of all the authors, the corresponding author states that there is no conflict of interest.

References

1. Brillouin L (1946) Wave Propagation in Periodic Structures, 1st edn. McGraw-Hill, Newyork
2. Hussein MI, Leamy MJ, Ruzzene M (2014) Dynamics of phononic materials and structures: historical origins, recent progress, and future outlook. Appl Mech Rev 66(4):040802
3. Maghami A, Mahmoud Hosseini SM (2022) Automated design of phononic crystals under thermoelastic wave propagation through deep reinforcement learning. Eng Struct 263:114385
4. Muhammad KJ, Lim CW (2022) Machine learning and deep learning in phononic crystals and metamaterials–A review. Mater Today Commun. https://doi.org/10.1016/j.mtcomm.2022.104606
5. Torrent D, Sanchez-Dehesa J (2010) Acoustic resonances in two-dimensional radial sonic crystal shells. New J Phys 12:073034
6. Arretche I, Matlack KH (2020) Effective phononic crystals for non-Cartesian elastic wave propagation. Phys Rev B 102:134308
7. Hvatov A, Sorokin S (2018) On application of the Floquet theory for radially periodic membranes and plates. J Sound Vib 414:15–30
8. Li L, He W, Jia Qi, Tong Z, Liu H, Li P, Li L (2022) Ultralow-frequency broadband characteristics of stepwise radial metamaterials. J Appl Phys 132:144902
9. Li L, Jia Q, Tong M, Li P, Zhang X (2021) Radial seismic metamaterials with ultra-low frequency broadband characteristics. J Phys D Appl Phys 54:505104
10. Yeh P, Yariv A (1978) Theory of Bragg fiber. J Opt Soc Am 68(9):1196–1201
11. Xu Y, Ouyang GX, Lee RK, Yariv A (2002) Asymptotic matrix theory of Bragg fibers. J Lightwave Technol 20(3):428–440
12. Kitagawa A, Sakai J (2009) Bloch theorem in cylindrical coordinates and its application to a Bragg fiber. Phys Rev A 80:033802
13. Hvatov A, Sorokin S (2023) On Unified Formulation of Floquet Propagator in Cartesian and Polar Coordinates. In: Dimitrovová Z, Biswas P, Gonçalves R, Silva T (eds) Recent trends in wave mechanics and vibrations. WMVC 2022. Mechanisms and machine science, vol 125. Springer International Publishing, Cham
14. Renno JM, Manconi E, Mace BR (2013) A finite element method for modelling waves in laminated structures. Adv Struct Eng 16:61–75
15. Manconi E, Sorokin SV, Garziera R, Quartaroli MM (2021) Free and forced wave motion in a two-dimensional plate with radial periodicity. Appl Sci 11:10948
16. Quartaroli MM, Manconi E, De Almeida FCL, Garziera R (2023) Vibration attenuation in plates with periodic annuli of different thickness. Recent trends in wave mechanics and vibrations. WMVC 2022. Mechanisms and machine science, vol 125. Springer International Publishing, Cham, pp 751–760
17. Hvatov A, Sorokin S (2015) Free vibrations of finite periodic structures in pass- and stop-bands of the counterpart infinite waveguides. J Sound Vib 347:200–217
18. Domadiya PG, Manconi E, Vanali M, Andersen LV, Ricci A (2016) Numerical and experimental investigation of stop-bands in finite and infinite periodic one-dimensional structures. J Vib Control 22:920–993
19. Germanos Cleante V, Brennan MJ, Paupitz Gonçalves PJ, Carneiro JP (2023) On the formation of a super attenuation band in a mono-coupled finite periodic structure comprising asymmetric cells. Recent trends in wave mechanics and vibrations. WMVC 2022. Mechanisms and machine science, vol 125. Springer International Publishing, Cham, pp 703–712
20. Hvatov A, Sorokin S (2019) Assessment of reduced-order models in analysis of Floquet modes in an infinite periodic elastic layer. J Sound Vib 440:332–345
21. Nielsen RB, Sorokin S (2015) Periodicity effects of axial waves in elastic compound rods. J Sound Vib 353:135–149

22. Manconi E, Mace BR (2009) Wave characterisation of cylindrical and curved panels using a finite element method. J Acoust Soc America 125:154–163
23. Manconi E, Mace BR, Garziera R (2013) The loss-factor of prestressed laminated curved panels and cylinders using a wave and finite element method. J Sound Vib 332:1704–1711
24. Waki Y, Mace BR, Brennan MJ (2009) Free and forced vibrations of a tyre using a wave/finite element approach. J Sound Vib 323:737–756
25. Fabro AT, Ferguson NS, Mace BR (2019) Wave propagation in slowly varying waveguides using a finite element approach. J Sound Vib 442:308–329
26. Auld BA (1990) Acoustic fields and waves in solids. Krieger Publishing Company, Malabar
27. Boukadia RF, Droz C, Ichchou MN, Desmet WA (2018) Bloch wave reduction scheme for ultrafast band diagram and dynamic response computation in periodic structures. Finite Elem Anal Des 148:1–12
28. Waki BR, Mace MJ (2009) Brennan, Numerical issues concerning the wave and finite element method for free and forced vibrations of waveguides. J Sound Vib 327:92–108